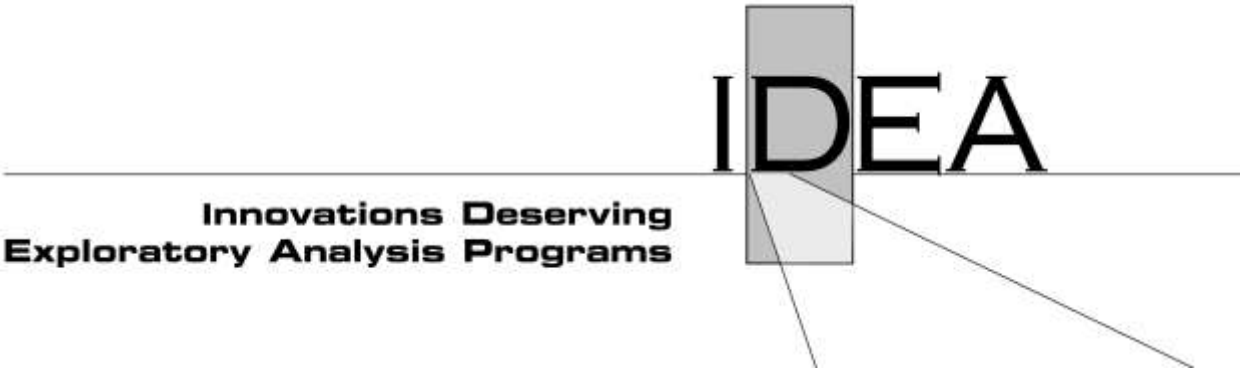

Safety IDEA Program

Determination of Longitudinal Stress in Rails

Final Report for
Safety IDEA Project 15

Prepared by:
Stefan Hurlebaus
Texas Transportation Institute
College Station, Texas

July 2011

TRANSPORTATION RESEARCH BOARD
OF THE NATIONAL ACADEMIES

INNOVATIONS DESERVING EXPLORATORY ANALYSIS (IDEA)
PROGRAMS MANAGED BY THE TRANSPORTATION RESEARCH BOARD

This Safety IDEA project was funded by the Safety IDEA Program, which focuses on innovative approaches for improving railroad safety and intercity bus and truck safety. The Safety IDEA Program is funded by the Federal Motor Carrier Safety Administration (FMCSA) and the Federal Railroad Administration (FRA) of the U.S. Department of Transportation. Any opinions, findings, conclusions, or recommendations expressed in this publication are those of the authors and do not necessarily reflect the views of the sponsors of the Safety IDEA program.

The Safety IDEA Program is one of three IDEA programs managed by TRB. The other two IDEA programs are listed below.

- The Transit IDEA Program, which supports development and testing of innovative concepts and methods for advancing transit practice, is funded by the Federal Transit Administration (FTA) as part of the Transit Cooperative Research Program (TCRP).
- The NCHRP Highway IDEA Program, which focuses on advances in the design, construction, and maintenance of highway systems, is funded as part of the National Cooperative Highway Research Program (NCHRP).

Management of the IDEA programs is coordinated to promote the development and testing of innovative concepts, methods, and technologies for these areas of surface transportation.

For information on the IDEA programs, look on the Internet at www.trb.org/idea, or contact the IDEA programs office by telephone at (202) 334-3310.

IDEA Programs
Transportation Research Board
500 Fifth Street, NW
Washington, DC 20001

Determination of Longitudinal Stress in Rails

Final Report

Safety IDEA Project 15

Prepared for

Safety IDEA Program

Transportation Research Board

National Research Council

Prepared by

Stefan Hurlebaus

Texas Transportation Institute
College Station, Texas

July 2011

CONTENTS

LIST OF FIGURES AND TABLES

ACKNOWLEDGEMENTS

The research reported herein was performed by the Texas Transportation Institute (TTI), College Station, and supported by the Safety Innovations Deserving Exploratory Analysis (Safety IDEA) Program and the Transportation Technology Center, Inc. (TTCI). The assistance and valuable input of the Safety IDEA program manager, Harvey Berlin, and the expert review panel for this project comprised of David Read (TTCI), Dr. Gary T. Fry (TTI), and Dr. Laurence J. Jacobs (Georgia Institute of Technology) is highly appreciated.

ABSTRACT

The objective of this project was to determine the longitudinal stress in rails, in order to reduce rail buckling due to temperature-induced stresses. Continuous welded rails (CWR) are typically long members which are susceptible to failure caused by temperature changes. Such rail temperature changes can cause considerable disruption to the rail network and, in the worst case, cause freight or passenger train derailment.

An important parameter in analysis of temperature induced stresses is the rail neutral temperature (RNT), defined as that rail temperature at which the net longitudinal force in the rail is zero. The objective of this project was to determine the longitudinal stress in rails using the polarization of Rayleigh surface waves, to reduce buckling and fracture.

This project developed a non-destructive procedure for monitoring the stress-free temperature in rails using the acoustoelastic effect of ultrasonic waves. Acoustoelasticity is the stress dependency of ultrasonic wave speed or polarization. Analytical models were developed to explain the relationship between the polarization of Rayleigh waves and the state of stress. Rayleigh waves were detected using a laser Doppler vibrometer (LDV). Furthermore, the polarization of Rayleigh waves is considered as a measure to identify applied stress.

EXECUTIVE SUMMARY

This research determined the rail neutral temperature (RNT) by using a non-destructive and non-labor intensive measurement technique of the rail stress using the polarization of Rayleigh waves. The relationship between the polarization of Rayleigh waves and the state of stress can be seen by an analytical model. The numerical simulation showed that the change of polarization of Rayleigh wave on residual stress is one order of magnitude higher than the change of Rayleigh wave speed. Additionally, a sensitivity analysis showed that the polarization of Rayleigh wave is more robust against uncertainties in material properties. The results revealed that Rayleigh wave polarization is more sensitive to longitudinal stress and more robust than the Rayleigh wave speed.

Further tasks as part of this project were done in order to implement this technology in the field. A preliminary laboratory experiment was conducted where the Rayleigh waves were generated in the rail using a wedge transducer. Then the polarization of Rayleigh waves in an unstressed rail was detected using a laser Doppler vibrometer (LDV) by measuring the out-of-plane as well as the in-plane component of the particle velocity. The results of the numerical simulation were verified with the preliminary experimental results. Further measurements were done in a stressed rail and the change in polarization of the Rayleigh wave was determined using a wedge transducer for generation and a LDV for the detection of ultrasonic waves. After a thorough evaluation, the concept was tested at Transportation Technology Center, Inc. (TTCI) facilities in Pueblo, CO, to transfer the developed technology to TTCI researches and Association of American Railroads (AAR) members. The results show that the polarization of Rayleigh wave changes with longitudinal stress. Knowing the longitudinal stress will prevent future buckling of the rail and reduce the number of derailments and increase railroad safety.

In a period of four years, 99 derailments occurred in the U.S resulting in about $38 million in damages. In total, there were ten times as many incidents of rail buckling due to temperature effects as those that resulted in derailments (Kish and Read).

The potential impacts of the application of this proposed technique on railroads are reduction of maintenance costs and increased safety. The non-destructive and non-labor intensive maintenance reduces the time needed to do inspections. The potential for cost savings in the U.S. railroad industry is considerable. This practical method gives the railroad industry the opportunity to check their rail lines more often and to correct the installation of the rails at the RNT, which can reduce buckling of the rail and decrease the number of train derailments.

CHAPTER 1

Background

Introduction

Continuous welded rails (CWR) are rails that are welded together to become long continuous members that are fixed at both ends. Using CWR will improve the convenience and reduce unneeded abrasion. There are also disadvantages in using CWR. Rail steel expands in hot weather and shrinks in cold weather, which could cause buckling and fracturing. Due to fixed ends, rails are restrained from expanding and shrinking. Hence, rails will experience a compressive stress in hot weather and they will undergo a tensile stress in cold conditions. The temperature at which the rails experience zero stress is called the rail neutral temperature (RNT). Large difference between the RNT and the surrounding temperature can cause the rails to buckle or fracture. Fig. 1 shows how rails could buckle due to a large difference between RNT and ambient temperature.

Fig. 1 – Buckling of Rails (*http://nisee.berkeley.edu*)

To prevent this problem, RNT needs to be set up to be in between the buckling and fracturing temperature. Kish and Samavedam (2005) identified that the RNT of rail steel could change due to several factors such as rail movement through fasteners. Moreover, the temperature of the rail can exceed the ambient temperature by around 30^{o}F

in hot weather, causing the rail steel to reach temperatures of 140^{o}F. This results in having a greater chance of rail buckling. For example, a CWR is installed at 90^{o}F (RNT = 90^{o}F). Consider that rail buckling happens at a temperature difference of 60^{o}F. Thus, rail will buckle when the temperature reaches to 150^{o}F. Due to rail movement through fastener, RNT drops to 50^{o}F. This change in RNT causes the rail to buckle when the temperature reaches 100^{o}F.

The example above shows how important it is to keep inspecting the RNT of CWR. Installing CWR at a "safe" region between buckling and fracturing temperatures does not guarantee that the rail will not buckle in the future. Hence, in order to prevent the rails from buckling or fracturing, RNT needs to be identified on a timely basis.

The objective of this research is to identify the longitudinal stress by using the polarization of Rayleigh waves in a non-destructive and non-labor intensive method. The ultrasonic wave will be generated by a transducer, and a laser Doppler vibrometer (LDV) is used to measure both the in-plane and out-of-plane velocity components of a Rayleigh wave as a function of applied stress (Hurlebaus and Jacobs, 2006). Once the longitudinal stress is identified and the ambient temperature is measured, RNT can then be calculated by using the relation between stress, ambient temperature, and the material properties given by

$$T_n = T_a - \frac{\sigma}{E\alpha} \quad , \tag{1.1}$$

where T_n is the rail neutral temperature, T_a is the ambient temperature, σ is the residual stress, E is Young's Modulus, and α is the thermal coefficient. The graph of this relation can be seen in Fig. 2. Once the RNT is determined, the conditions of the rails can be known, and decisions can be made regarding whether re-installing the entire rail is necessary to increase safety.

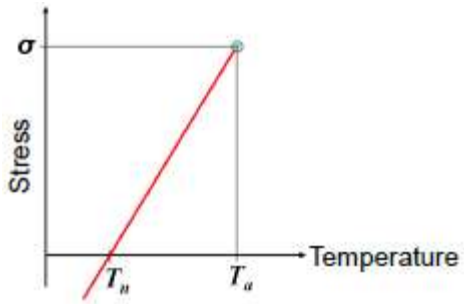

Fig. 2 – Rail Neutral Temperature

Methods of Residual Stress Measurements

There are several methods that railroad industries have been using to determine the longitudinal stress in rails. Each of these techniques has disadvantages. Using traditional techniques, stress can be measured by cutting the rail, measuring the gap, calculating the RNT, and re-welding the rail. This method is a destructive measurement, labor intensive, and costly.

The VERSE method, shown in Fig. 3, measures the stress non-destructively. In this method, the rail is unclipped and lifted, a set of loads are then applied, the displacement is monitored, and the rail is re-clipped. Although this method is a non-destructive, this technique is labor and measurement intensive; thus, it is time consuming and costly.

Fig. 3 – VERSE equipment *(http://www.railway-technology.com)*

Egle and Bray (1979) use the acoustoelastic effect on longitudinal wave speed using contact transducers. The disadvantages of this method are that a very precise measurement of propagation distance is needed to determine the longitudinal wave speed, and the correlation between longitudinal wave speed and residual stress is low.

The d'Stresen technique (Read, 2007) identifies that the vibration amplitude of a rail is proportional to the longitudinal force in the rail, but only when the rail is under tension. Also, this technique is a contact measurement technique; thus, it cannot be applied while trains are running. Damljanovic and Weaver (2005) investigated the technique of measuring the stress in rails using the principle of sensitivity of bending rigidity to stress. This technique measures the bending wave number in the rail for the unstressed and stressed case. The drawback of this technique is that it requires a very high precision equipment to do the experiment.

Acoustoelastic Effect

The determination of material properties such as material constants, flaw detection, or applied stress can be obtained by various types of ultrasonic waves. Crecraft (1962, 1967) found that acoustoelasticity or the acoustoelastic effect is a functional technique for determining material properties. Using the correlation of the stress dependence of wave velocities in solids, the dependency of ultrasonic waves on stress is called the acoustoelastic effect.

Murnaghan (1951) developed a nonlinear elastic theory for isotropic materials. This theory introduces third-order elastic (TOE) constants which help explain the acoustoelastic effect with a theoretical model. The theory was applied by Toupin and Berstein (1961) to an elastically deformed material to observe the propagation behavior of acoustic waves. Pao and Garmer (1985) extended this theory to an orthotropic media.

The acoustoelastic effect is very small. Special techniques are required to measure the stress-induced velocity changes. Crecraft (1967) uses the sing-around technique to measure the acoustoelastic effect. This technique uses one or two transducers that are

coupled to the specimen. The first transducer generates a pulse to be received by the second transducer. This pulse is then used to retrigger the sending transducer. The frequency of this echoing pulse is related to the travel time of the ultrasonic wave. Hughes and Kelly (1953) used the pulse-echo technique to measure stress-induced velocity changes. In this technique, the time a pulse travels through a specimen is measured.

Hirao et al. (1981) did research on the acoustoelastic effect on Rayleigh waves in a homogeneous isotropic material. It was found that Rayleigh waves are non-dispersive and the velocity change is linear under a uniform stress. Duquennoy et al. (1999, 2001) used Rayleigh waves to analyze residual stresses. Fig. 4 shows the change of Rayleigh wave polarization with applied stress.

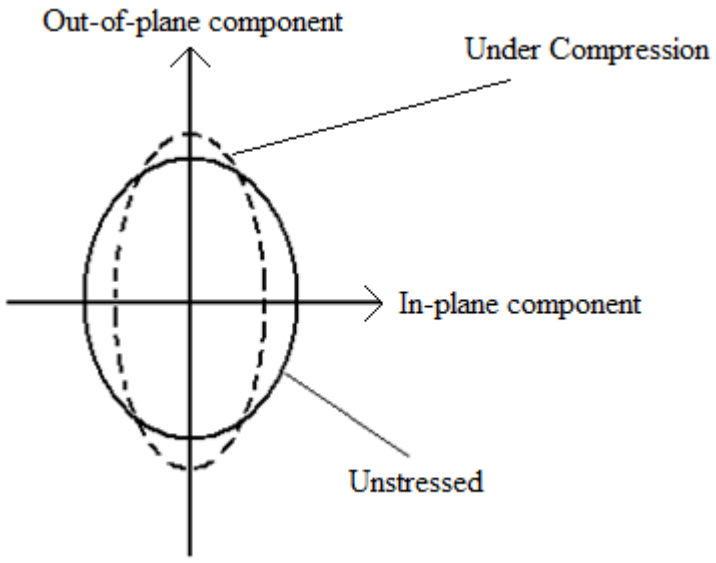

Fig. 4 – Change of Rayleigh wave polarization under applied stress

The proposed method is a non-destructive and non-labor intensive measurement technique (Hurlebaus 1996, 2002b). The change in polarization of the Rayleigh wave is measured instead of the longitudinal wave speed; therefore, information on the propagation distance is not needed (Junge, 2003, Junge et al., 2006). This technique is also applicable on rails under tension or compression.

CHAPTER 2
Research Approach

The following investigations were done as part of the current project:

1: Literature Review

The research team compiled a literature review to fully document the state of practice on estimating the rail stress. The team will continue the literature review throughout the duration of the project to identify new information and to identify possible issues and areas of improvement.

2: Analytical Model

This task developed an analytical model that predicts the relationship between the polarization of a Rayleigh wave and the state of stress. This relationship is used to measure applied stress. The analytical model is based on the equations of motion for a pre-stressed body.

3: Numerical Simulation

The numerical simulation for the problem concerning Rayleigh waves in a pre-stressed medium was performed. First, an iterative algorithm that solves the relevant analytical equations was developed followed by an analysis of the numerical problem. Moreover, a sensitivity analysis was performed that investigates the influence of uncertainties in the third order elastic constants on the wave speed and the polarization.

4: Preliminary Experiment

The purpose of this preliminary experiment was focused on how to generate Rayleigh waves in rails using a wedge transducer. Then the polarization of Rayleigh waves in an unstressed rail were detected using a laser Doppler vibrometer (LDV) by measuring the out-of-plane as well as the in-plane component of the particle velocity.

5: Model Updating

Verification of the results of the numerical simulation with the preliminary experimental results was done. This provides the opportunity to account for any uncertainties in material properties of the rail or for any geometrical uncertainties.

6: Experiment

Measurements were done in TTCI facilities at Pueblo, CO. by using hydraulic clamps to do a tension test. The experiment was done by using a wedge transducer for Rayleigh wave generation, and the change in polarization of the Rayleigh wave between stressed and unstressed rail steel was determined.

CHAPTER 3
Analytical Model of Elastic Waves

This chapter provides descriptions on the subject of wave propagation, Rayleigh waves, states of a solid body, and third-order constant (TOE). These subjects help in understanding the analytical model discussed in the next chapter.

Wave Propagation

The equation of motion of an elastic solid is governed by the Lame-Navier equation given by

$$\frac{\partial T_{mn}}{\partial x_n} + \rho f_m = \rho \frac{\partial^2 u_m}{\partial t^2} \ , \tag{3.1}$$

where ρ symbolizes the density of the material, f_m are the internal body forces, x_n denotes the direction in the coordinate system shown in Fig. 5, u_m is the displacement in the x_m direction, and T_{mn} denotes the stress tensor in the generalized Hooke's Law given as

$$T_{mn} = C_{mnpq} \frac{\partial u_p}{\partial x_q} \ . \tag{3.2}$$

By substituting Eq. (3.2) to Eq. (3.1) and neglecting the body forces, the equation of motion can be written as

$$C_{mnpq} \frac{\partial^2 u_p}{\partial x_n \partial x_q} = \rho \frac{\partial^2 u_m}{\partial t^2} \ , \tag{3.3}$$

where C_{mnpq} is the second order stiffness tensor given by

$$C_{mnpq} = \lambda \delta_{mn} \delta_{pq} + \mu (\delta_{mp} \delta_{nq} + \delta_{mq} \delta_{nq}) \ . \tag{3.4}$$

Notation λ and μ in Eq. (3.4) denote the Lame's constants, and δ is the Kronecker delta. Lame's constants can be expressed in terms of Young's Modulus E, and Poisson's ratio υ

$$\mu = \frac{E}{2(1+\upsilon)}, \qquad \text{and} \qquad \lambda = \frac{E\upsilon}{(1+\upsilon)(1-2\upsilon)} \quad . \tag{3.5}$$

By plugging Eq. (3.4) into Eq. (3.3), the equation of motion becomes

$$\mu\nabla^2 u_m + (\lambda+\mu)\frac{\partial}{\partial x_m}\left(\frac{\partial u_n}{\partial x_n}\right) = \rho\frac{\partial^2 u_m}{\partial t^2}, \tag{3.6}$$

where ∇ denotes the nabla operator $\nabla^2 = \frac{\partial^2}{\partial x_1^2} + \frac{\partial^2}{\partial x_2^2} + \frac{\partial^2}{\partial x_3^2}$.

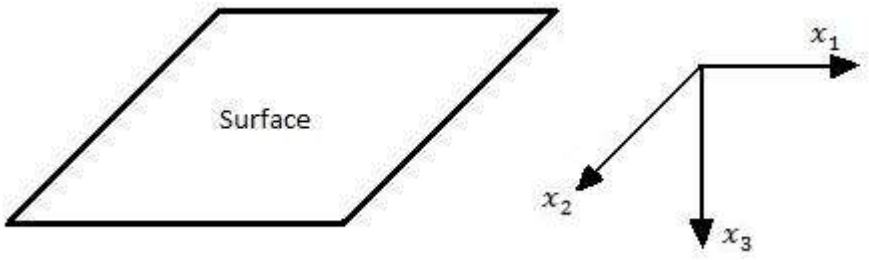

Fig. 5 – Coordinate system

To satisfy the equation of motion in Eq. (3.6), the displacement vector can be expressed in the form of

$$\boldsymbol{u} = f(\boldsymbol{x}\cdot\boldsymbol{p} - ct)\boldsymbol{d}, \tag{3.7}$$

where c is the wave speed, $\boldsymbol{p}$ represents the unit propagation, $\boldsymbol{x}$ is the location of the displacement vector, and $\boldsymbol{d}$ is the unit displacement vectors.

Longitudinal waves have polarization vectors parallel to the displacement vector, or $\boldsymbol{p} = \boldsymbol{d}$. Conversely, shear waves have polarization vector perpendicular to the displacement vector, or $\boldsymbol{p}\cdot\boldsymbol{d} = 0$. By inserting each of these characteristics into Eq. (3.7) and then plugging the result into Eq. (3.6), the wave speed can be determined as

$$c_l^{\,2} = \frac{\lambda + 2\mu}{\rho}, \tag{3.8}$$

$$c_S^{\,2} = \frac{\mu}{\rho}, \tag{3.9}$$

where c_l and c_S are the longitudinal wave speed and the shear wave speed, respectively.

Eq. (3.7) can be uncoupled in terms of longitudinal and shear waves by utilizing the Helmholtz decomposition. The displacement in uncoupled terms can be expressed in terms of a scalar function ϕ and a vector field $\boldsymbol{\psi}$

$$\boldsymbol{u} = \nabla\phi + \nabla\times\boldsymbol{\psi} \quad . \tag{3.10}$$

By substituting Eq. (3.10) back into Eq. (3.6), the uncoupled equations are

$$\nabla^2\phi = \frac{1}{c_l^2}\frac{\partial^2\phi}{\partial t^2} \qquad \text{and} \qquad \nabla^2\boldsymbol{\psi} = \frac{1}{c_s^2}\frac{\partial^2\boldsymbol{\psi}}{\partial t^2} \quad . \tag{3.11}$$

Rayleigh Wave

A Rayleigh wave is a non dispersive wave that propagates on the free surface of a solid. It was first found by Lord Rayleigh in 1885 (Hurlebaus, 2002a). The particles of a Rayleigh wave travel in a counterclockwise direction with an elliptic trajectory along the free surface and then change to a clockwise direction as the depth increases. A Rayleigh wave's amplitude decays as a function of depth (coordinate x_3), and the motion does not depend on the coordinate x_2. Fig. 6 shows the trajectory plot of a Rayleigh wave particle.

In Rayleigh waves, the scalar function and vector field can be assumed to be

$$\phi = F(x_3)e^{ik(x_1 - ct)}$$

$$\boldsymbol{\psi} = G(x_3)e^{ik(x_1 - ct)} \quad , \tag{3.12}$$

where F and G are functions of x_3, and k is the wave number given by $k = 2\pi/\lambda$. Plugging Eq. (3.12) into Eq. (3.11) gives the surface wave motion

$$\phi = A_1 e^{-kqx_3} e^{ik(x_1 - ct)}$$

$$\psi = B_1 e^{-ksx_3} e^{ik(x_1 - ct)}, \tag{3.13}$$

where A_1 and B_1 are arbitrary constants and

$$q = \sqrt{1 - \left(\frac{c_R}{c_l}\right)^2} \qquad\qquad s = \sqrt{1 - \left(\frac{c_R}{c_s}\right)^2} \ .$$

The boundary conditions require that stress is equal to zero at $x_3 = 0$. Substitution of this boundary condition into Eq. (3.13) yields the Rayleigh characteristic equation

$$\left(2 - \frac{c_R^2}{c_s^2}\right)^2 - 4\sqrt{\left(1 - \frac{c_R^2}{c_l^2}\right)}\sqrt{\left(1 - \frac{c_R^2}{c_s^2}\right)} = 0 \ . \tag{3.14}$$

Eq. (3.14) has six roots, whose values depend only on Poisson's ratio υ for a given elastic media. Victorov (1966) showed that for arbitrary values of υ corresponding to real media ($0 < \upsilon < 0.5$), Eq. (3.14) has only one such root. An approximate expression for the Rayleigh wave velocity c_R is given by Graff (1991)

$$\frac{c_R}{c_S} = \frac{0.87 + 1.12\upsilon}{1 + \upsilon} . \tag{3.15}$$

This propagation velocity is smaller than those of the body waves. As the velocity c_R is independent of the wavelength, the wave propagation is non dispersive. The propagation of a Rayleigh wave is depicted in Fig. 6. It can be shown that an arbitrary point will move with elliptical motion as the Rayleigh wave passes by. Most of the energy in the Rayleigh wave is present in the depth of one wavelength from the surface. Due to this skin effect, the Rayleigh wave has great potential for detection of faults at the surface of structures. Furthermore, the Rayleigh wave causes the most damage during an earthquake because it carries more energy at the surface than either longitudinal or shear waves.

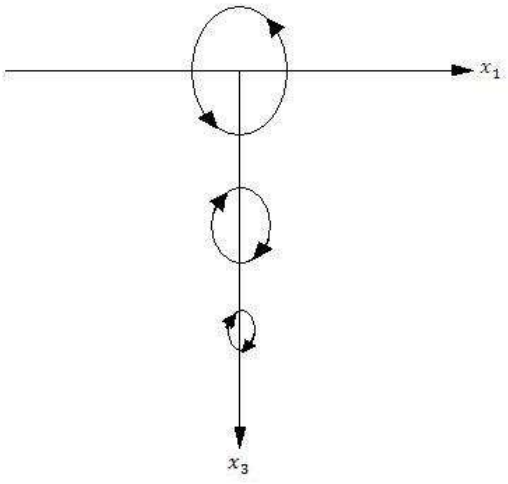

Fig. 6 – Trajectory plot for various depths (Junge, 2003)

Rose (1999) derived the displacements of the Rayleigh waves that satisfy the boundary conditions to be

$$\begin{aligned} u_1 &= A(re^{-qx_3} - 2sqe^{-sx_3})e^{ik(x_1 - c_R t)} \\ u_3 &= -iAq(-re^{-qx_3} + 2e^{-sx_3})e^{ik(x_1 - c_R t)} \end{aligned}, \tag{3.16}$$

where $r = 2 - \left(c_R / c_S\right)^2$ and $A = kB_1 / 2q$. Plotting the displacement of u_1 and u_3 gives the ellipse shape of particle motion. Polarization of a Rayleigh wave can be described as the ratio of maximum displacements along the ellipse's axes given by

$$\prod = \frac{u_1}{u_3} \quad . \tag{3.17}$$

Lamb Waves

Consider a double-bounded medium that has two parallel surfaces in close proximity. Disturbances are constrained to move between the two surfaces, and therefore the system behaves as a waveguide. Of interest is the case where the top and bottom surfaces are traction-free. For this set of boundary conditions, waves known as Lamb waves propagate in the plate. Depicted in Fig. 7 are the displacement profiles for the first Lamb modes. The essence of the analysis is that standing waves are established in the transverse direction, while propagating waves travel in the lengthwise direction. Consider

a plane, harmonic Lamb wave propagating along the positive x_1-direction in a plate with thickness *h*. The scalar and vector potentials can be expressed as

$$\phi = \left[C_1 \sin\left(\sqrt{k^2 - k_L^2}\, x_3\right) + C_2 \cos\left(\sqrt{k^2 - k_L^2}\, x_3\right) \right] e^{ik(x_1 - ct)} \tag{3.18}$$

$$\psi = \left[D_1 \sin\left(\sqrt{k^2 - k_S^2}\, x_3\right) + D_2 \cos\left(\sqrt{k^2 - k_S^2}\, x_3\right) \right] e^{ik(x_1 - ct)}, \tag{3.19}$$

where k_L and k_S are the wave numbers of the longitudinal and shear waves, respectively, C_1, C_2, D_1 and D_2 are arbitrary constant. Implementation of the boundary conditions $\sigma_{33} = \sigma_{13} = 0$ at the free surface $x_3 = \pm h/2$ leads, after some manipulation, to the well-known Rayleigh-Lamb frequency equations

$$\frac{\tanh\left(\frac{h}{2}\sqrt{k^2 - k_S^2}\right)}{\tanh\left(\frac{h}{2}\sqrt{k^2 - k_L^2}\right)} = -\frac{4k^2\sqrt{k^2 - k_S^2}\sqrt{k^2 - k_L^2}}{(2k^2 - k_S^2)^2} \tag{3.20}$$

for the symmetric case and

$$\frac{\tanh\left(\frac{h}{2}\sqrt{k^2 - k_S^2}\right)}{\tanh\left(\frac{h}{2}\sqrt{k^2 - k_L^2}\right)} = -\frac{(2k^2 - k_S^2)^2}{4k^2\sqrt{k^2 - k_S^2}\sqrt{k^2 - k_L^2}} \tag{3.21}$$

for the antisymmetric case. For the symmetric mode shapes, the displacement u_1 is symmetric about the axis $x_3 = 0$; and for the antisymmetric mode shapes the displacement u_1 is antisymmetric about the axis $x_3 = 0$ (Fig. 7). At a spatially-fixed plate cross section, the amplitude of a mode shape will oscillate with angular frequency ω as wavefronts travel through the cross-section with velocity *c*. Eq. (3.20) and Eq. (3.21) can be expressed in terms of ω and *c* using the relationship $k = \omega / c$.

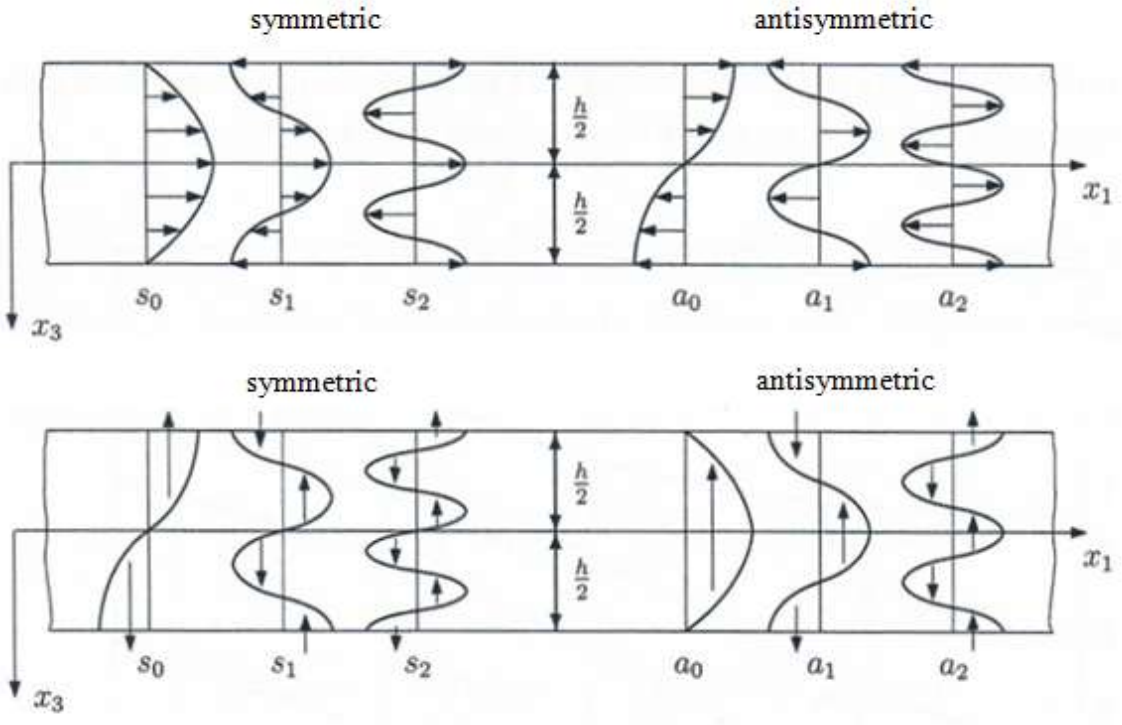

Fig. 7 – Symmetric and antisymmetric components of the u_1, u_3 displacements (*Hurlebaus, 2005*)

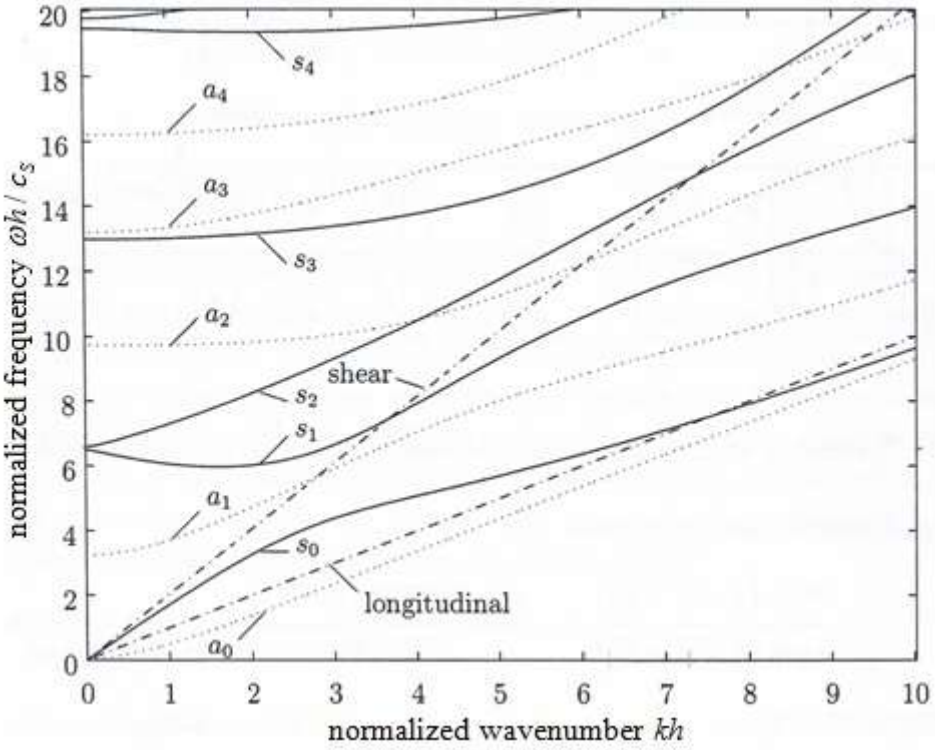

Fig. 8 – Theoretical dispersion curves calculated from Rayleigh-Lamb frequency equations (*Hurlebaus, 2005*)

For a given frequency, these equations can be solved for the unknown velocity of the mode in question. A plot of ω vs. c (or ω vs. k) for a particular mode is known as a dispersion curve. Fig. 8 shows typical dispersion curves in the normalized (ω, k) domain for Lamb waves together with dispersion curves for the longitudinal and shear wave. The symmetric Lamb modes are called $s_0, s_1, s_2, \ldots$ and the antisymmetric modes are called $a_0, a_1, a_2, \ldots$. Lamb waves are – as opposed to Rayleigh waves – dispersive, whereby the propagation velocity of a specific Lamb mode depends upon its oscillation frequency. For a given (ω, k) combination, the mode shape can be computed using Eq. (3.11), Eq. (3.18), and Eq. (3.19). Fig. 7 shows the in-plane and out-of-plane displacements u_1, u_3 for symmetric as well as for antisymmetric Lamb waves.

States of a Solid Body

Natural, initial, and final states are different states that can be found in a solid. A solid body is in the *natural state* when there is no residual stress and strain in the body. In practice, such state does not exist in a solid material. Solid materials experience stresses from fabrication processes or external loading that leads to deformation. When material undergoes such stress, it is said to be in its *initial state.* The *final state* takes place when the material undergoes additional deformation due to other stress applied on the body such as the propagation of ultrasonic wave. Fig. 9 shows the arrangement of the three states of a body in the Cartesian coordinate system.

Pao et al. (1984) refers the position vectors of the natural, initial, and final states to be $\boldsymbol{\xi}$, $\boldsymbol{X}$, and $\boldsymbol{x}$ respectively. The relationship of the displacements of these states can be expressed as

$$\boldsymbol{u}^i(\boldsymbol{\xi}) = \boldsymbol{X} - \boldsymbol{\xi} \tag{3.22}$$

$$\boldsymbol{u}^f(\boldsymbol{\xi}) = \boldsymbol{x} - \boldsymbol{\xi} \tag{3.23}$$

$$\boldsymbol{u}(\boldsymbol{\xi}) = \boldsymbol{x} - \boldsymbol{X} = \boldsymbol{u}^f - \boldsymbol{u}^i \quad , \tag{3.24}$$

where superscript i and f stand for initial and final, respectively.

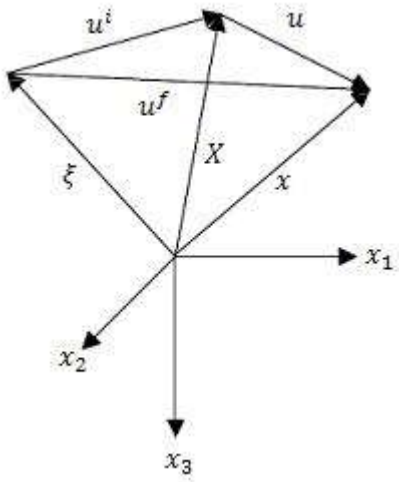

Fig. 9 – Coordinate system of natural, initial, and final states of a body (*Junge, 2003*)

Third-Order Elastic (TOE) Constant

The existence of elastic constants is very important in determining the stress state of the material using the ultrasonic wave method. The second order elastic constant can be found by using the linear theory of elasticity. When there is an applied stress in the material, the second order elastic constants cannot explain the change in ultrasonic wave velocities. Thus, a higher order of nonlinear elasticity theory was established. This theory introduces the second-order Lame constant and the third-order elastic constant. For isotropic materials, the second- and third-order elastic constants can be expressed in the forms

$$C_{\alpha\beta\gamma\delta} = \lambda\delta_{\alpha\beta}\delta_{\gamma\delta} + \mu(\delta_{\alpha\gamma}\delta_{\beta\delta} + \delta_{\alpha\delta}\delta_{\beta\gamma}), \tag{3.25}$$

and

$$\begin{aligned} C_{\alpha\beta\gamma\delta\varepsilon\eta} = {} & \upsilon_1\delta_{\alpha\beta}\delta_{\gamma\delta}\delta_{\varepsilon\eta} + \upsilon_2[\delta_{\alpha\beta}(\delta_{\gamma\varepsilon}\delta_{\delta\eta} + \delta_{\gamma\eta}\delta_{\delta\varepsilon}) + \delta_{\gamma\delta}(\delta_{\alpha\varepsilon}\delta_{\beta\eta} + \delta_{\beta\varepsilon}\delta_{\alpha\eta}) + \\ & \delta_{\varepsilon\eta}(\delta_{\alpha\gamma}\delta_{\beta\delta} + \delta_{\alpha\delta}\delta_{\beta\gamma})] + \upsilon_3[\delta_{\alpha\gamma}(\delta_{\beta\varepsilon}\delta_{\delta\eta} + \delta_{\beta\eta}\delta_{\delta\varepsilon}) + \\ & \delta_{\beta\delta}(\delta_{\alpha\varepsilon}\delta_{\gamma\eta} + \delta_{\alpha\eta}\delta_{\gamma\varepsilon}) + \delta_{\alpha\delta}(\delta_{\beta\varepsilon}\delta_{\gamma\eta} + \delta_{\beta\eta}\delta_{\gamma\varepsilon}) + \\ & \delta_{\beta\gamma}(\delta_{\alpha\varepsilon}\delta_{\delta\eta} + \delta_{\alpha\eta}\delta_{\delta\varepsilon})], \end{aligned} \tag{3.26}$$

where υ_1, υ_2, and υ_3 are the Toupin and Bernstein (1961) notation of TOE.

CHAPTER 4

Findings and Applications

Equation of Motion for a Pre-stressed Body

The state of stress at a given point as a function of $\boldsymbol{X}$ is defined by the Cauchy stress tensor, $\boldsymbol{t}^i(\boldsymbol{X})$. While the Piola-Kirchhoff stress tensor, $\boldsymbol{T}^i(\boldsymbol{\xi})$, describes the state of stress at the same given point in the natural configuration. Both of these tensors are related by

$$t^i_{JK} = \left|\frac{\partial \boldsymbol{X}}{\partial \boldsymbol{\xi}}\right|^{-1} \frac{\partial X_K}{\partial \xi_\beta}\frac{\partial X_J}{\partial \xi_\alpha} T^i_{\alpha\beta} \quad . \tag{4.1}$$

The relation of the final state of stress of these two tensors can also be found by using the same analogy given by

$$t^f_{ij} = \left|\frac{\partial \boldsymbol{x}}{\partial \boldsymbol{\xi}}\right|^{-1} \frac{\partial x_i}{\partial \xi_\alpha}\frac{\partial x_j}{\partial \xi_\beta} T^f_{\alpha\beta} = \left|\frac{\partial \boldsymbol{x}}{\partial \boldsymbol{X}}\right|^{-1} \frac{\partial x_i}{\partial \xi_K}\frac{\partial x_j}{\partial \xi_L} T^f_{KL} \quad , \tag{4.2}$$

and the stress change from the initial to final state is defined by

$$T_{JK} = T^f_{JK} - t^i_{JK}$$

$$T_{\alpha\beta} = T^f_{\alpha\beta} - t^i_{\alpha\beta} . \tag{4.3}$$

Given these basic explanations, Pao et al. (1984) derives the equation of motion as

$$\frac{\partial}{\partial X_J}\left[(\delta_{IK} t^i_{JL} + \hat{C}_{IJKL})\frac{\partial u_K}{\partial X_L}\right] = \rho^0(1-\varepsilon^i_{NN})\frac{\partial^2 u_i}{\partial t^2} , \tag{4.4}$$

where $\hat{C}_{IJKL}$ represents the adapted stress tensor of a pre-stressed body. Both the adapted stress tensor and initial strain are respectively given by

$$\begin{aligned}\hat{C}_{IJKL} = {} & \lambda\delta_{IJ}\delta_{KL} + \mu(\delta_{IK}\delta_{JL} + \delta_{IL}\delta_{JK}) + [(-\lambda + \upsilon_1)\delta_{IJ}\delta_{KL} + \\ & (-\mu + \upsilon_2)(\delta_{IK}\delta_{JL} + \delta_{IL}\delta_{JK})]\varepsilon^i_{MM} + 2(\lambda + \upsilon_2)(\varepsilon^i_{IJ}\delta_{KL} + \varepsilon^i_{KL}\delta_{IJ}) + \\ & 2(\mu + \upsilon_3)(\varepsilon^i_{IK}\delta_{JL} + \varepsilon^i_{IL}\delta_{JK} + \varepsilon^i_{JK}\delta_{IL} + \varepsilon^i_{JL}\delta_{IK})\end{aligned} \tag{4.5}$$

,

and the initial strain, ε_{KL}^{i}, is determined by

$$\varepsilon_{KL}^{i} = \frac{-\lambda}{2\mu(3\lambda+2\mu)}\delta_{KL}t_{NN}^{i} + \frac{1}{2\mu}t_{KL}^{i} \ . \tag{4.6}$$

Rayleigh Waves in Pre-stressed Bodies

Assuming that the initial stress is homogeneous, Eq. (4.4) can be simplified into

$$(\delta_{IK}t_{JL}^{i} + \hat{C}_{IJKL})\frac{\partial u_K}{\partial X_J X_L} = \rho(1-\varepsilon_{NN}^{i})\frac{\partial^2 u_I}{\partial t^2} \ . \tag{4.7}$$

In this chapter, the displacement field is selected to be in the form

$$\boldsymbol{u} = \boldsymbol{a}e^{ik(X_1+pX_3-c_R t)}, \tag{4.8}$$

where $\boldsymbol{a}$ represents the displacement vector, and p is the decay parameter. The form of this displacement field represents the propagation of a Rayleigh wave where its motion decays exponentially with increasing depth. Plugging Eq. (4.8) into Eq. (4.7) yields the equation

$$\{p^2\hat{\boldsymbol{S}} + p(\hat{\boldsymbol{R}} + \hat{\boldsymbol{R}}^T) + \hat{\boldsymbol{Q}} - \rho_0(1-\varepsilon_{NN}^{i})c_R^2\boldsymbol{I}\}\boldsymbol{a} = 0,$$

or

$$\{\boldsymbol{D}(c_R, p)\}\boldsymbol{a} = 0 \ , \tag{4.9}$$

where $\boldsymbol{I}$ is the identity matrix, and $\hat{\boldsymbol{S}}$, $\hat{\boldsymbol{R}}$, and $\hat{\boldsymbol{Q}}$ are given by

$$\hat{S}_{IK} = \hat{C}_{I3K3} \qquad \hat{R}_{IK} = \hat{C}_{I1K3} \qquad \hat{Q}_{IK} = \hat{C}_{I1K1} + \delta_{IK}t_{11}^{i} \ . \tag{4.10}$$

The displacement vector $\boldsymbol{a}$ can be determined by solving for null space of $\boldsymbol{D}$ for each p_i, which can be solved by setting

$$\left\|\boldsymbol{D}(c_R, p)\right\| = 0 \quad . \tag{4.11}$$

The decay parameters, p_i, solved in Eq. (4.11) consist of three pairs of complex conjugate roots for p. Once the displacement vectors $\boldsymbol{a}_i$ are determined, the

displacement field can be written as a linear combination of the single solutions using the matrix notation

$$\boldsymbol{u} = \boldsymbol{A}\boldsymbol{G}(X_3)\,\boldsymbol{f}e^{ik(X_1-ct)}\ , \tag{4.12}$$

where $\boldsymbol{f}$ is a vector that consists of factors for the linear combination, $\boldsymbol{A} = \left[\boldsymbol{a}_1, \boldsymbol{a}_2, \boldsymbol{a}_3\right]$, and

$$\boldsymbol{G}(X_3) = \begin{bmatrix} e^{ikp_1X_3} & 0 & 0 \\ 0 & e^{ikp_2X_3} & 0 \\ 0 & 0 & e^{ikp_3X_3} \end{bmatrix}. \tag{4.13}$$

The boundary condition of the state of stress for Rayleigh waves in a pre-stressed body is given by

$$T_{12} = \hat{C}_{I2KL}\frac{\partial u_K}{\partial X_L} = 0 \text{ , at } X_3 = 0\ . \tag{4.14}$$

Plugging Eq. (4.12) into the boundary condition yields

$$(\hat{\boldsymbol{R}}^T\boldsymbol{A} + \hat{\boldsymbol{S}}\boldsymbol{A}\boldsymbol{P})\,\boldsymbol{f} = 0,$$

or

$$\left(\boldsymbol{B}(c_R, p)\right)\boldsymbol{f} = 0\ , \tag{4.15}$$

where

$$\boldsymbol{P} = \begin{bmatrix} p_1 & 0 & 0 \\ 0 & p_2 & 0 \\ 0 & 0 & p_3 \end{bmatrix}. \tag{4.16}$$

For a non-trivial solution of Eq. (4.15), the matrix $\boldsymbol{B}$ must equal to zero or

$$\left\|\boldsymbol{B}(c_R, p)\right\| = 0\quad , \tag{4.17}$$

and the vector $\boldsymbol{f}$ can be found by solving for the null-space of $\boldsymbol{B}$.

The polarization of Rayleigh waves is defined as the ratio of maximum displacements in the x_1 and x_3 directions on the free surface. The polarization of Rayleigh wave is given by

$$\prod = \frac{(\boldsymbol{Af})_1}{(\boldsymbol{Af})_2} \ . \tag{4.18}$$

Algorithm for Numerical Simulation

The numerical simulation to the problem of Rayleigh wave propagation is done by using Matlab software. This simulation determines the changes of Rayleigh wave speed, c_R, and polarization of the Rayleigh wave, $\Delta\prod$, due to residual stresses. Junge (2003) has arranged the iterative algorithm as follows:

1. Identify an initial Rayleigh wave speed, c_{R0}. This can be done by using Eq. (3.14). The longitudinal and shear wave speeds can be determined by using Eq. (3.8) and Eq. (3.9). Poisson's ratio is needed to perform this calculation, and it can be found by

$$\upsilon = \frac{\lambda}{2(\lambda + \mu)} \tag{4.19}$$

2. Plug in the wave speed from step 1 into Eq. (4.9) and solve for p_i that makes the determinant of $\boldsymbol{D}$ equal to zero.
3. For each value of p_i, solve for the null-space, $\boldsymbol{a}_i$, in Eq. (4.9) and construct the matrix $\boldsymbol{A}$.
4. Use the values of p to construct the matrix $\boldsymbol{P}$ in Eq. (4.16).
5. Construct matrix $\boldsymbol{B}$ as stated in Eq. (4.15).
6. If the determinant of matrix $\boldsymbol{B}$ is not equal to zero, use another value of c_{R0} and start all over again from step 2.
7. The value of c_{R0} that satisfies the boundary condition is the Rayleigh wave speed, c_R, due to the residual stress.
8. Solve for the null-space, $\boldsymbol{f}$, in Eq. (4.15)
9. Compute the polarization vector using Eq. (4.18)

Relative Change of Rayleigh Waves on Residual Stress

The relative change of the wave speed and polarization with stress are very small in rail steel. Many publications use the relative change of wave speed instead of the absolute value of the wave speed and polarization because of this reason. Moreover, the acoustoelastic effect can be clearly visualized by using the relative change. The relative change of Rayleigh wave speed is given by

$$\Delta c_R = \frac{c_R - c_{R0}}{c_{R0}} \quad , \tag{4.20}$$

and the relative change of Rayleigh wave polarization is

$$\Delta \prod = \frac{\prod - \prod_0}{\prod_0} \quad . \tag{4.21}$$

The numerical simulation in this chapter uses the properties of rail steel found by Egle and Bray (1976) that are shown in Table 1.

Table 1 – Material properties of rail steel

ρ (kg/m^3)	λ (GPa)	μ (GPa)	υ_1 (GPa)	υ_2 (GPa)	υ_3 (GPa)
7799	110.7	82.4	-96	-254	-181

Rail steel has yield strength of 450 MPa. This simulation runs the analysis ranging from a compressive force of -440 MPa to a tensile force of 440 MPa. Fig. 10(a) shows the results of the simulation on the change of wave speed due to residual stress. This plot shows that there is a linear relation between them and is given by

$$\Delta c_R = k^c \cdot t_{11}^i \quad , \tag{4.22}$$

where k^c is a wave speed proportionality factor.

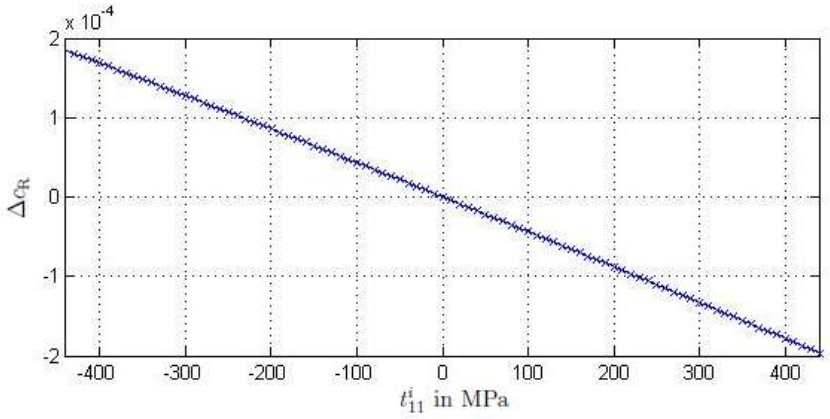

(a) Change of wave speed on residual stress

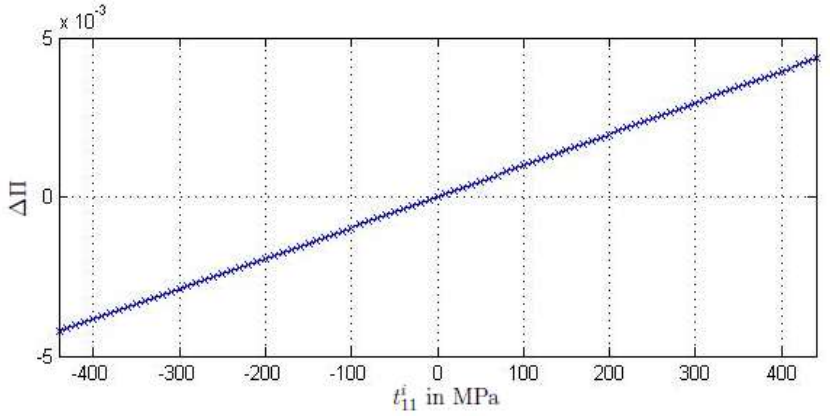

(b) Change of Rayleigh wave polarization on residual stress

Fig. 10 – The change in wave speed (a) and the change in Rayleigh wave polarization (b) due to residual stress for rail steel

Similarly, Fig. 10(b) also shows that there is linear relation between $\Delta\prod$ and t_{11}^i given by

$$\Delta\prod = k^p \cdot t_{11}^i \quad , \tag{4.23}$$

where k^p is the polarization proportionality factor. Both the k^c and k^p are used to measure the sensitivity of the Rayleigh wave speed and the polarization of the Rayleigh wave, respectively. Based on the simulations, the proportionality factors are determined to be

$$k^c = \text{-4.3 x } 10^{-7} / \text{ MPa} \qquad \text{and} \qquad k^p = 9.8 \text{ x } 10^{-6} / \text{ MPa}$$

Sensitivity Analysis

In the previous section, TOE constants are assumed to remain unchanged in the simulation. In reality, the values of TOE constants have some uncertainties. Eagle and Bray (1976) identified an estimated error of the TOE constants for rail steel to be about 3% - 4%. Smith et al. (1966) found the uncertainties of TOE constants for austenitic Steel Hecla ATV to be more than 20%. As can be seen for the examples, sensitivity analysis on the TOE constants needs to be done to discover the change of wave speed and polarization of Rayleigh waves against uncertainties for any case. In contrast, Lame constants can be determined precisely and, hence, can be assumed to remain constant.

Assuming an uncertainty of 20% in rail steel properties, the scale of relative change of Rayleigh wave speed and polarization of Rayleigh wave can be seen in Fig. 11. This plot shows that the experimental results may vary within the shaded area since the values of TOE constants are not known exactly.

The proportionality factors are investigated in this sensitivity analysis to have a better understanding of the uncertainties in TOE constants. Table 2 shows the percentage differences of maximum and minimum proportionality factors to the real value. It is seen that the values of k^p are greater than the values of k^c by about one order of magnitude. This means that the change of Rayleigh wave polarization on residual stress is higher than the change of wave speed, thus, it is easier to be analyzed. In addition, the percentage difference against uncertainties of k^p is much smaller than k^c, meaning that the Rayleigh wave polarization is more robust. These are the two main reasons why Rayleigh wave polarization is used instead of the Rayleigh wave speed in this research.

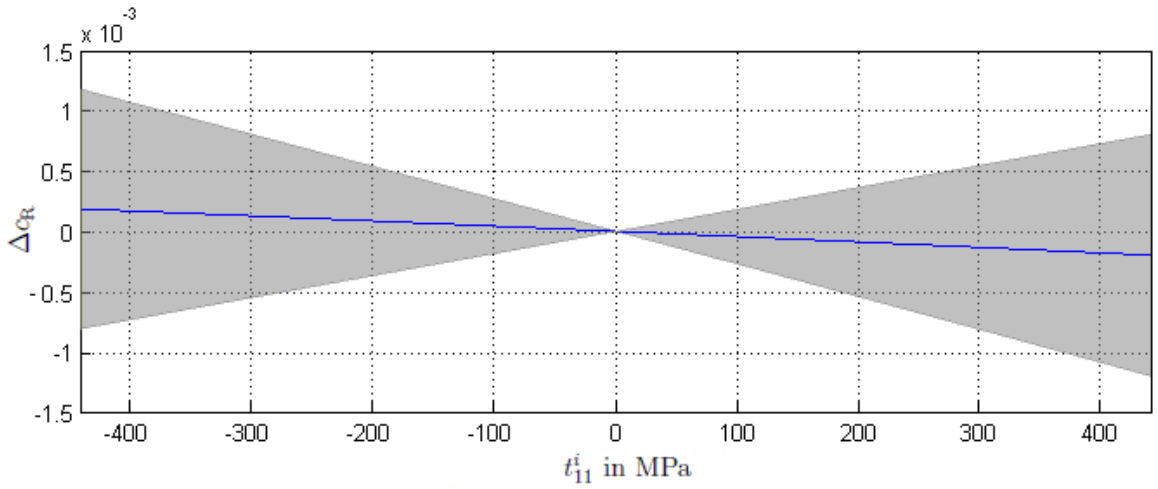

(a) Change of wave speed against uncertainties

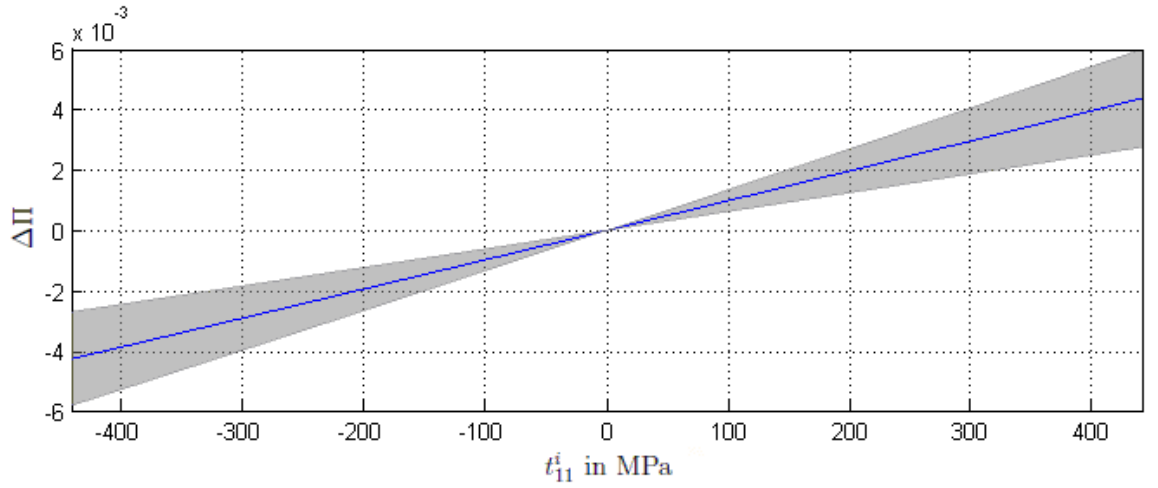

(b) Change of polarization of Rayleigh wave against uncertainties

Fig. 11 – The change in wave speed (a) and the change in Rayleigh wave polarization (b) against uncertainties. The changes are within the shaded area.

Table 2 - Variations of TOE Constants [GPA] and Proportionality Factors

	υ_1	υ_2	υ_3	k^c	% diff	k^p	% diff
Min	-115.2	-304.8	-217.2	-2.69E-06	519.65%	1.34E-05	36.78%
Avg	-96	-254	-181	-4.34E-07		9.76E-06	
Max	-76.8	-203.2	-144.8	1.82E-06	-519.64%	6.17E-06	-36.77%

Rayleigh Wave Polarization

The values of Rayleigh wave polarization are obtained by dividing the displacements in the x_1 direction by the displacements in the x_3 direction. These values can also be plotted against each other to visualize the shape of particle motion. Fig. 12 shows the change in the shape in particle motion between unstressed and stressed rail steel.

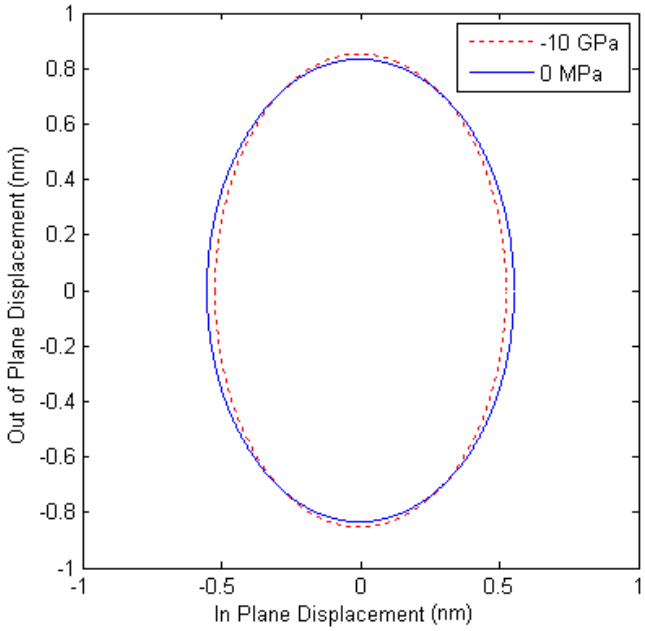

Fig. 12 – Trajectory plot of particle motion for unstressed and stressed rail steel

Frequency Range

Ideally, the Rayleigh wave can only propagate along an elastic half-space. In this research, the Rayleigh wave is generated to propagate on the web of rail steel. The web of the rail steel itself is a plate like structure. Hence, a frequency range where the Rayleigh wave theory can be applied needs to be determined.

This propagation of Rayleigh wave itself is a superposition of the first antisymmetric and symmetric Lamb modes as explained by Victorov (1966). In a previous section of this report, Lamb waves are explained in more detail.

Masserey et al. (2008) investigated the propagation of Rayleigh waves in aluminum plates. The propagation of Rayleigh waves starts on the surface and gradually transfers to the other side of the plate, and then transfers back to the surface from which it started. The distance of that one whole cycle is called the beat length, calculated as

$$L = \frac{2\pi}{k_{A0} - k_{S0}} \quad , \tag{4.24}$$

where k_{A0} and k_{S0} are the wave numbers of A_0 and S_0 modes respectively. Fig. 13 shows the wave number dispersion curve in a rail steel.

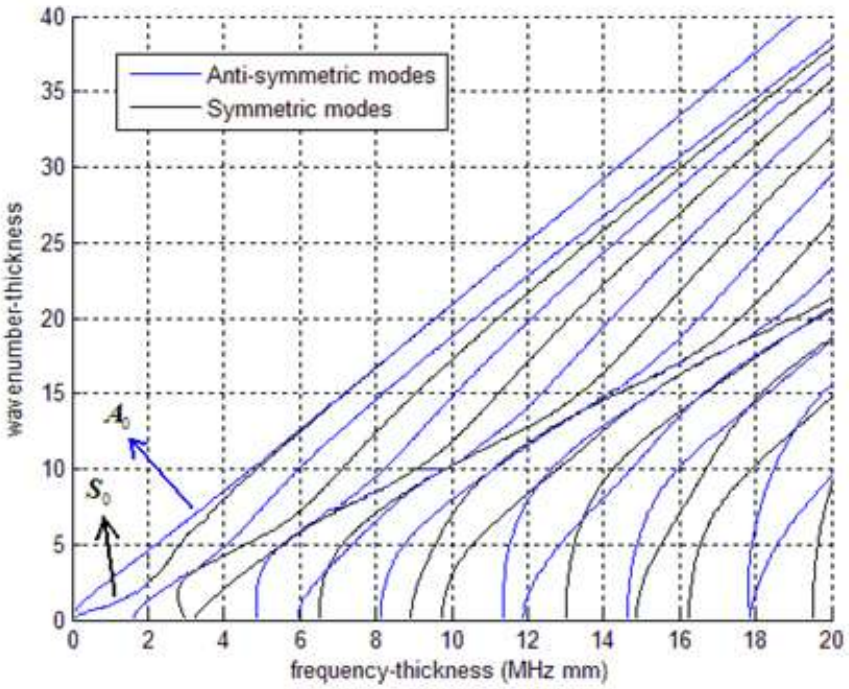

Fig. 13 – Rail steel dispersion

If the beat length approaches infinity, the amplitude of the Rayleigh wave is only decaying with distance. This could only be achieved when the denominator term $(k_{A0} - k_{S0})$ approaches zero. In the dispersion curve chart (Fig. 13), increments in frequency-thickness results in decrements in the denominator term.

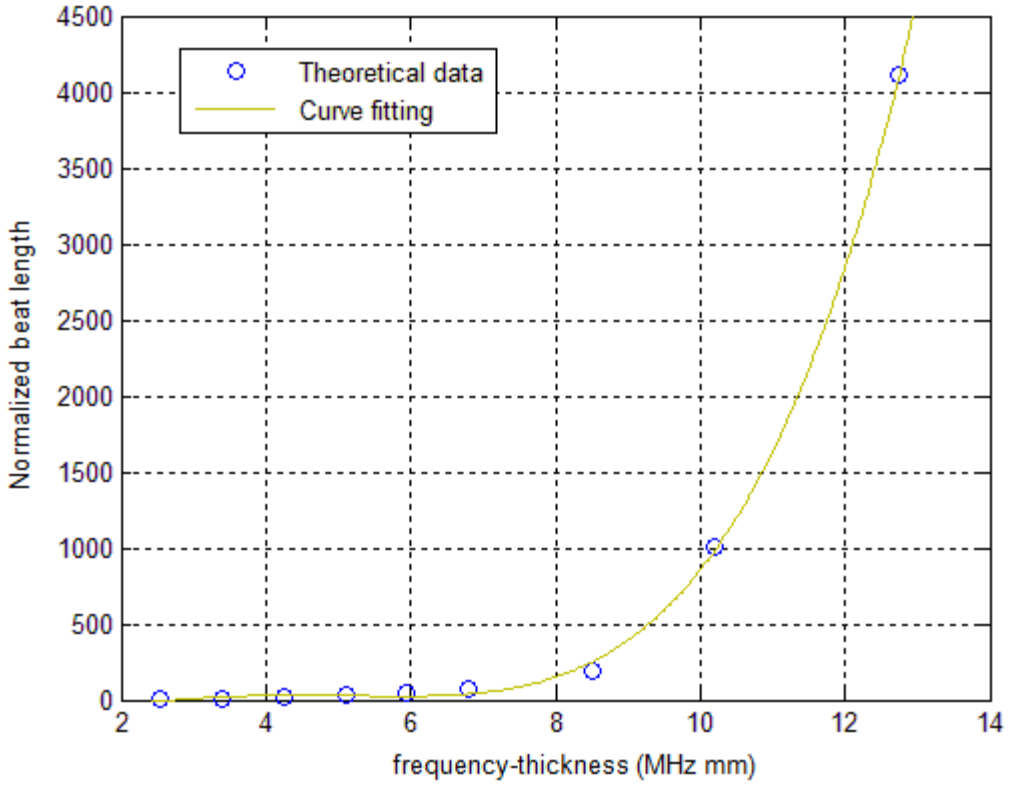

Fig. 14 – Normalized beat length L/h vs. frequency thickness fh with h = 17 mm

To determine the best frequency range, normalized beat length L/h is plotted against frequency-thickness fh in Fig. 14. We can safely make an assumption that for a frequency-thickness greater than 10 MHz mm, the beat length approaches infinity, hence the amplitude of the Rayleigh wave is not dependent on distance. For a web thickness h of 17 mm (as used in the experiment), a frequency range of greater than 600 kHz is appropriate.

A test was conducted to find out how frequency range affects the attenuation of Rayleigh wave propagation. The test consisted of finding the out-of-plane amplitude of the rail for 45 different locations starting at Location A (look Fig. 15) and moving in increments of 0.4 cm further from transducer to Location B. This test was done with excitation frequencies of 200 kHz and 1 MHz. Fig. 16 shows the plots of out-of-plane displacement amplitude vs. distance from transducer. With the excitation frequencies of 200 kHz, the amplitudes attenuated up to a certain distance, and then started to intensify again. While with the excitation frequencies of 1 MHz, the amplitudes of the Rayleigh

wave decayed with distance and did not intensify for a long distance, which is what we would want in this experiment. With these results, the experiment will be done with excitation frequency greater than 600 kHz.

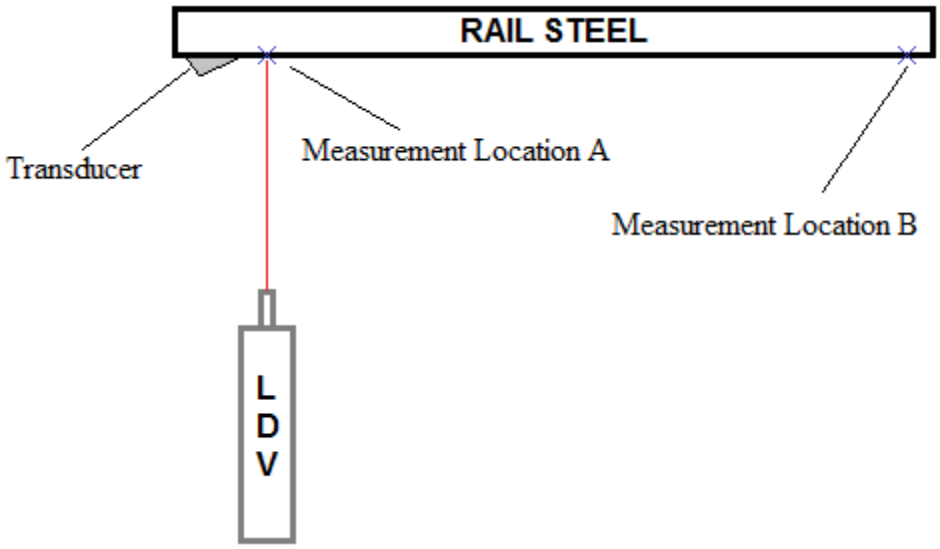

Fig. 15 – Experimental setup for finding frequency range

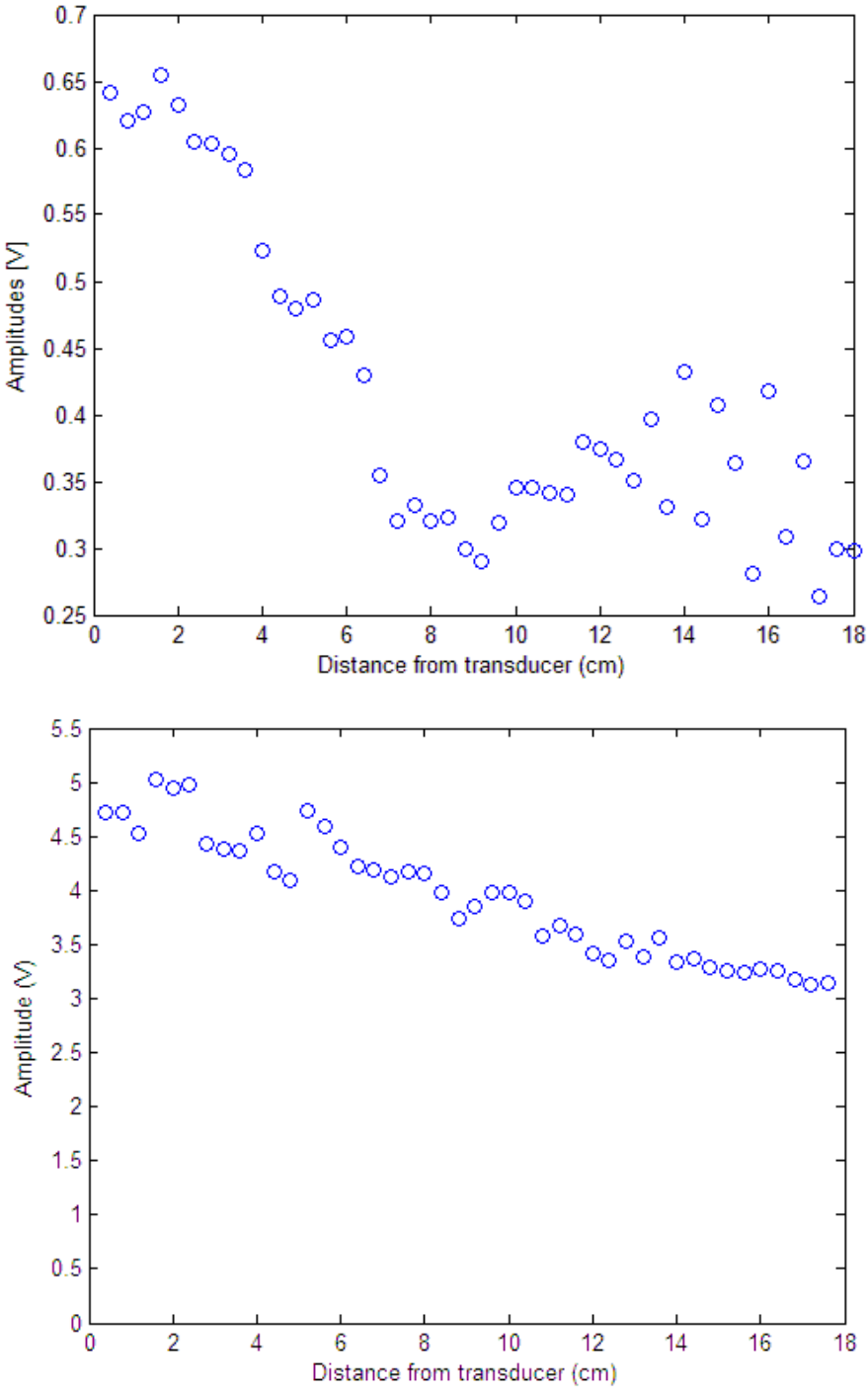

Fig. 16 – Out-of-plane displacement amplitude vs. distance from transducer with 200 kHz excitation (top) and 1 MHz excitation (bottom)

CHAPTER 5

Experimental Setup and Results

Generation of Rayleigh Waves Using the Wedge Technique

Wedge technique allows a longitudinal transducer to be mounted on a wedge and to be rotated to a certain angle of θ_w to generate Rayleigh waves only. Fig. 17 shows the picture of a transducer mounted on a wedge that is used in the experiments.

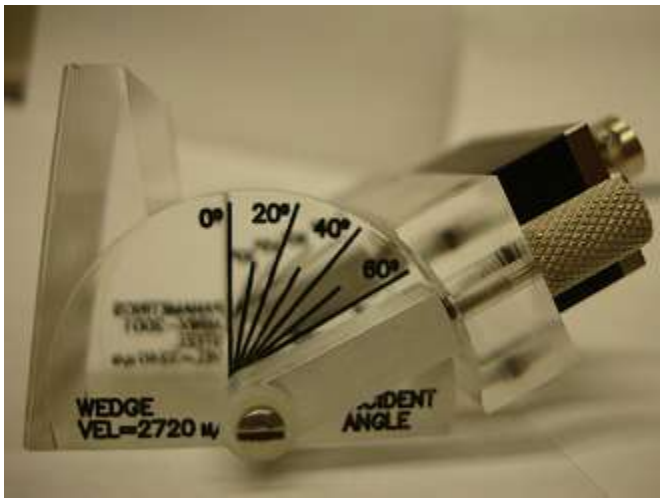

Fig. 17 – Wedge transducer

By looking at Fig. 18, the incident angle θ_w can be calculated as

$$\frac{\sin\theta_w}{\sin\theta_R} = \frac{c_l^{(1)}}{c_R^{(2)}} = \frac{\lambda_l^{(1)}}{\lambda_R^{(2)}} \tag{5.1}$$

where the superscript (1) and (2) denotes the 1st material (the wedge, which is a plexiglass) and the 2nd material (rail steel), respectively, and θ_R is the refracted angle with $\theta_R = 90^o$, which leads to

$$\sin\theta_w = \frac{c_l^{(1)}}{c_R^{(2)}} \tag{5.2}$$

Eq. (5.2) proves that this technique only works if the Rayleigh wave speed of the specimen, $c_R^{(2)}$, is greater than the longitudinal wave speed of the plexiglass, $c_l^{(1)}$.

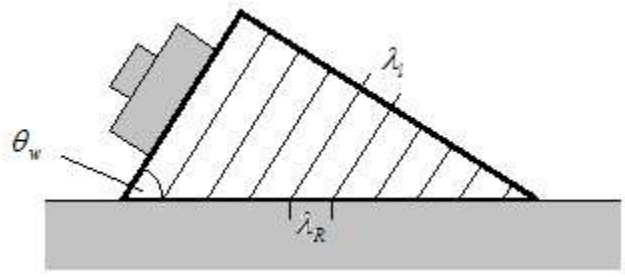

Fig. 18 – Wedge transducer (*Junge,2003*)

The Rayleigh wave speed for rail steel is about 3000 m/s, and the longitudinal wave speed of the plexiglass wedge is 2720 m/s. By using Eq. (5.2), the incident angle θ_w needed to generate a Rayleigh wave on rail steel is 65^o.

Theoretically, when the incident angle θ_w is used on the longitudinal transducer to generate a Rayleigh wave, shear waves and longitudinal waves will not be transmitted by the transducer. This perfectly mode conversion from longitudinal wave to Rayleigh wave is one advantage of using a wedge technique. This is true because Rayleigh wave speed is always smaller than the shear and longitudinal waves speed. By utilizing the incident angle in Eq. (5.2), the angle of the transmitted shear and longitudinal waves would be

$$\sin\theta_l = \sin\theta_w \cdot \frac{c_l^{(2)}}{c_l^{(1)}} = \frac{c_l^{(2)}}{c_R^{(2)}} > 1 \tag{5.3}$$

$$\sin\theta_s = \sin\theta_w \cdot \frac{c_s^{(2)}}{c_l^{(1)}} = \frac{c_s^{(2)}}{c_R^{(2)}} > 1 \tag{5.4}$$

Eq. (5.3) and Eq. (5.4) prove that both shear and longitudinal wave speed would not be transmitted since the solutions for both angles do not exist. Another advantage of the wedge technique is that it is valid for all frequency ranges without changing the incident angle. The perfect mode conversion also applies for its waveforms. For example,

a longitudinal wave with sinusoidal waveform will stay as a sinusoidal waveform when it is mode converted to a Rayleigh wave.

Experimental Setup

In the preliminary experiment, a wedge transducer is used to generate Rayleigh wave on 1 ft rail steel. The setup for this experiment can be seen in Fig. 19. In generating the signal, a function generator is used to set up the excitation frequency and number of burst cycle. The experiment uses a burst signal of 10-cycle. The excitation frequency ranges between 800 kHz to 1 MHz to determine the best measurement frequency of the overall setup.

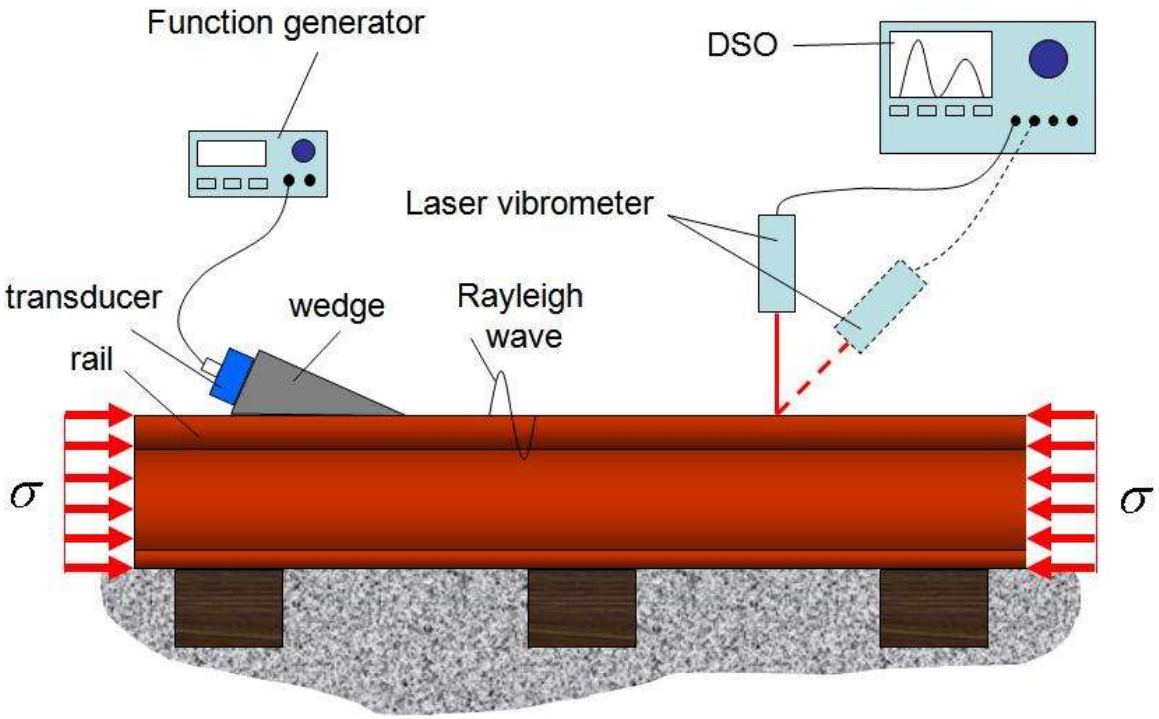

Fig. 19 – Experimental setup using transducer

The transducer used in this experiment is a Centrascan series C401 from Panametrics with a center frequency of 1 MHz. This transducer is attached to an angle beam Panametrics wedge ABWX-2001. The transducer is set up at an incident angle θ_w of 65^o as specified in the previous section.

The Rayleigh wave detection is done by using a laser Doppler vibrometer (LDV). The basic concept of this vibrometer is to detect the frequency shift or phase shift of the laser light that is reflected from a vibrating surface. This Doppler frequency (or phase) shift is then used to determine the surface velocity of the particles. Kil et al. (1998) explained more about LDV system in details.

A Digital Storage Oscilloscope (DSO) Tektronix TDS 3034B is used to record the data captured by the LDV. The signals are averaged five-hundred-twelve times to increase the signal-to-noise-ratio (SNR).

Experimental Procedure

To obtain the in-plane and out-of-plane component, measurements from two different angles are necessary. The first measurement is done by setting the LDV perpendicular to the rail to measure the out-of-plane velocity. The second measurement is done under an angle of θ from the axis of the web of the rail. Figure 20 shows the sketch of experimental setup for the out-of-plane measurement and the off-angle measurement. In order to obtain the in-plane component of the measured signals the relation

$$\begin{Bmatrix} V_{IP} \\ V_{OP} \end{Bmatrix} = \frac{1}{\sin(\theta_a - \theta_b)} \begin{bmatrix} -\sin(\theta_b) & \sin(\theta_a) \\ \cos(\theta_b) & -\cos(\theta_a) \end{bmatrix} \begin{Bmatrix} V_a \\ V_b \end{Bmatrix} \tag{5.5}$$

is used, where V_{IP}, and V_{OP} are the in-plane and out-of-plane velocity components, respectively, θ_a, and θ_b are the angles measured from the axis of the web of the rail, and V_a, and V_b are the velocity components measured under the angle of θ_a and θ_b, respectively.

The first measurement is done by setting the LDV perpendicular (θ_a from the axis of the web) to the rail to measure the out-of-plane velocity. The second measurement is

done by placing two mirrors in the path of the laser with the intention of getting the measurement θ_b from the axis of the web of the rail. Mirror 1 was fixed on the table, while Mirror 2 was fixed on a translation stage. Using the translation stage helps in getting reproducible results since Mirror 2 can be placed to a desired location with the accuracy of 0.01 mm.

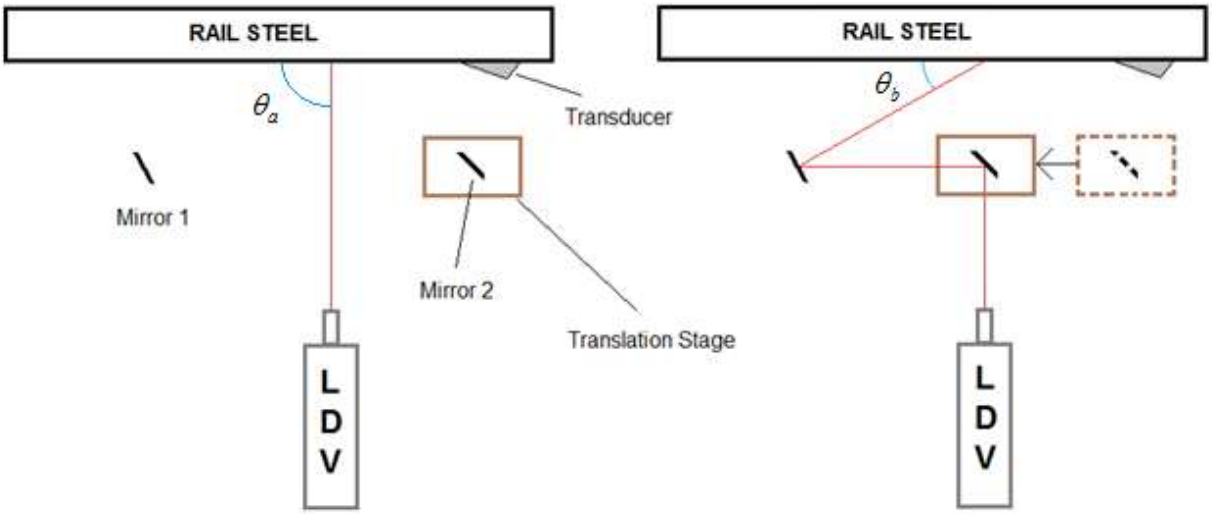

Fig 20 - Sketch of out-of-plane (left) and off-angle (right) measurement

Experimental Results in Unstressed Rail Steel

In this experiment, an excitation frequency of 800 kHz is used, and the sampling frequency is set to 250 MHz. The experiment was done by using angles of $\theta_a = 90^o$ and $\theta_b = 50^o$.

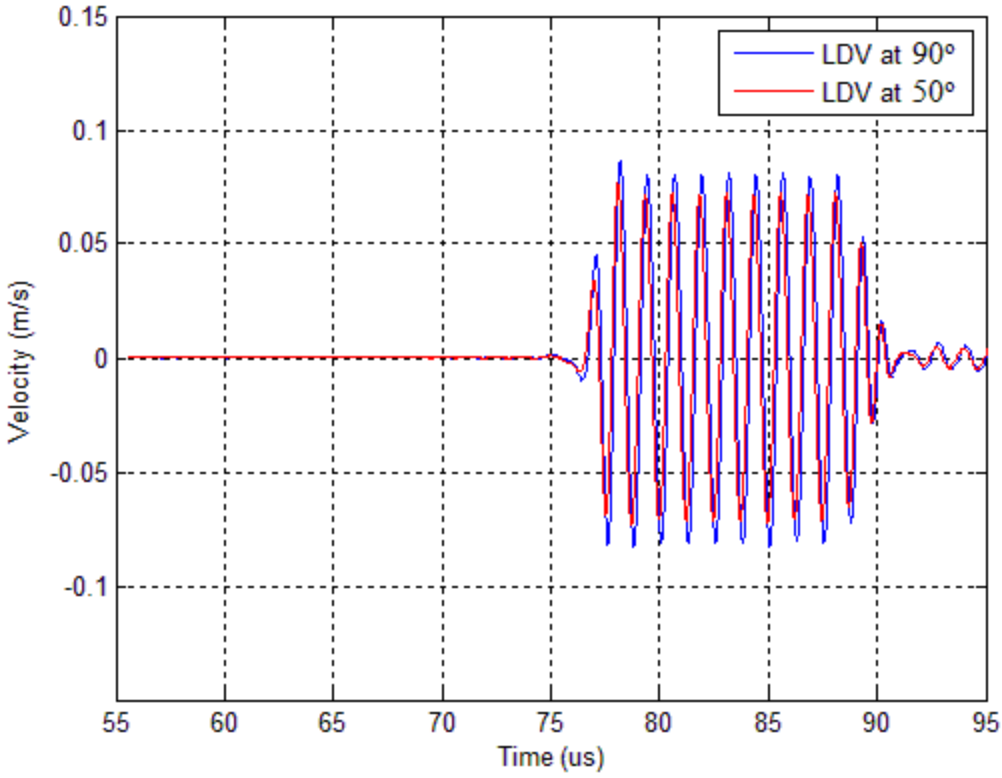

Fig. 21 – Raw data in time domain

The time domain signal of raw data can be seen in Fig. 21. As expected, only the Rayleigh wave was identified in the plot due to the wedge technique. After analyzing the raw data, the in-plane and out-of-plane displacement components are obtained, and the plot can be seen in Fig. 22.

The in-plane and out-of-plane displacement components are plotted against each other and can be seen in Fig. 23. As expected, the shape of the Rayleigh wave polarization is in a form of an ellipse.

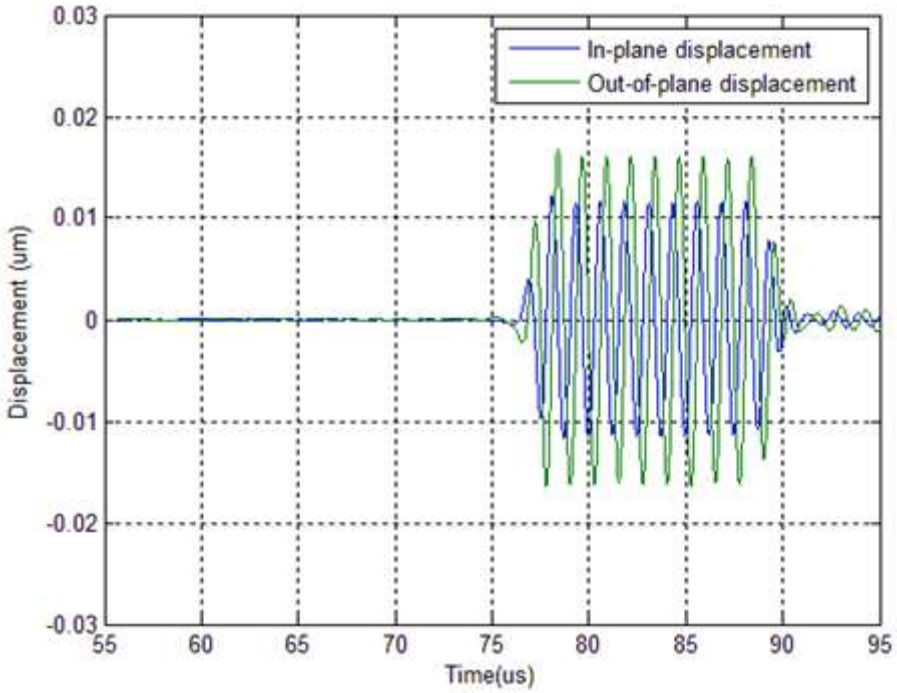

Fig. 22 – In-plane and out-of-plane displacements in time domain

This experiment is performed 10 times, and the results can be seen in Table 3. The total average value of Rayleigh wave polarization of these 10 experiments was calculated to be 0.7242, with a standard deviation of 0.0134 and coefficient of variation of 1.86%. The theoretical Rayleigh wave polarization is 0.6631. Therefore the experimental results are in good agreement with the theoretical predictions.

The length of the rail used in this experiment might be a factor in the difference between the experimental result and theoretical value. The specimen used in this experiment was a 1-foot rail steel. With this size of rail, end effects could appear, which will disturb the Rayleigh wave signal.

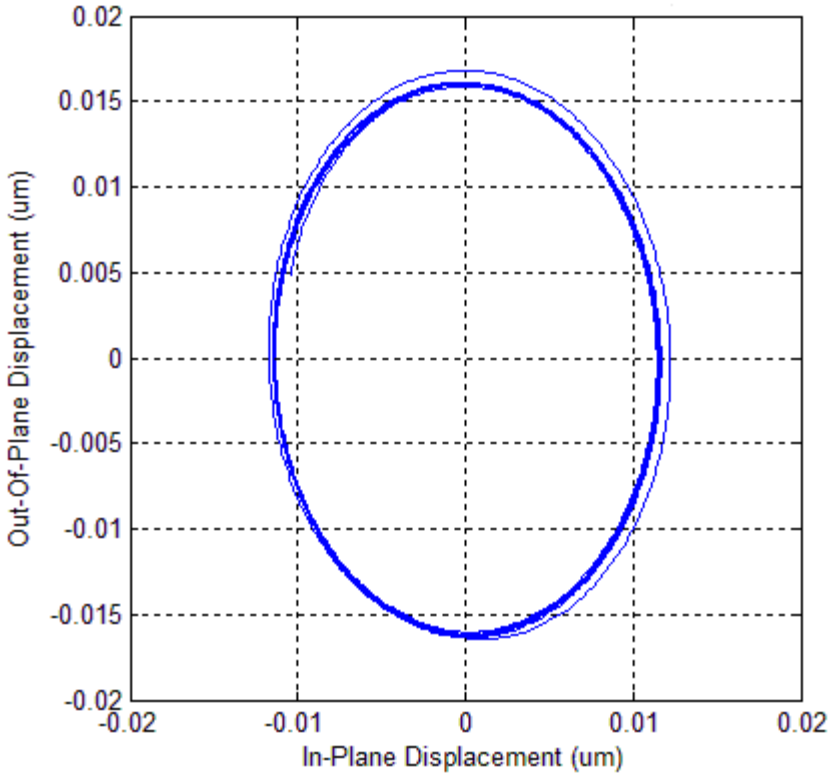

Fig. 23 – Polarization of Rayleigh wave

Table 3 – Polarization values of 10 experiments with 800 kHz excitation frequency and 250 MHz sampling frequency

Experiment No.	Polarization Value	Average	Standard Deviation	Coefficient of Variation
1	0.7160	0.7242	0.0134	1.86%
2	0.7061			
3	0.7560			
4	0.7271			
5	0.7269			
6	0.7313			
7	0.7205			
8	0.7139			
9	0.7184			
10	0.7253			

Experimental Results in Stressed Rail Steel

The stressed test was done at Transportation Technology Center, Inc. (TTCI) facilities in Pueblo, CO, and different rail steel was used. The condition of the rail was used with a length of 15 ft. The experiment was also set up just like in Fig. 20. The transducer was driven by a burst signal of ten cycles with excitation frequency of 800 kHz and a sampling frequency of 250 MHz. The signal was amplified using an RF amplifier to improve the signal-to–noise ratio. For this experiment, angles of θ_a = 90^o and θ_b = 30^o were chosen. The specimen is stressed by using a hydraulic rail puller attached to the rail. Fig. 24 depicts the experimental setup with the rail puller, the ultrasonic transducer, the LDV and the instrumentation.

Fig. 24 – Experimental setup at TTCI facilities

The rail surface was not appropriate for the measurement because the rust on the rail disturbed the reflection of the laser back to LDV. Therefore a reflective tape was used

on the rail surface. Once the out-of-plane measurement and 30^{o} angle measurement were acquired, the data was processed using MATLAB, and the ratio between in-plane and out-of-plane component was calculated to get the Polarization of Rayleigh wave.

The experiment was done on the rail under different loads. During the compression test, some of the rail puller clamps slipped. The rail experienced bending and torsional moment during compression, causing the rail to "jump" when the compression load exceeded a specific value. This "jump" caused the movement of the wedge transducer. Furthermore, due to the slipping of the rail puller the stress in the rail was not constant over time. The current setup requires the measurement at two different angles. With the restriction of a single LDV, these measurements cannot be done simultaneously. Hence, the data of the compression test are excluded in this report.

For each load case, three sets of repeating measurements were performed, and the average of the polarization values was calculated. Fig 25 shows the dependence between the normalized polarization of the Rayleigh wave and the normalized load. It can be seen that the polarization of Rayleigh waves increases with increasing tension load. These results agree with the analytical results.

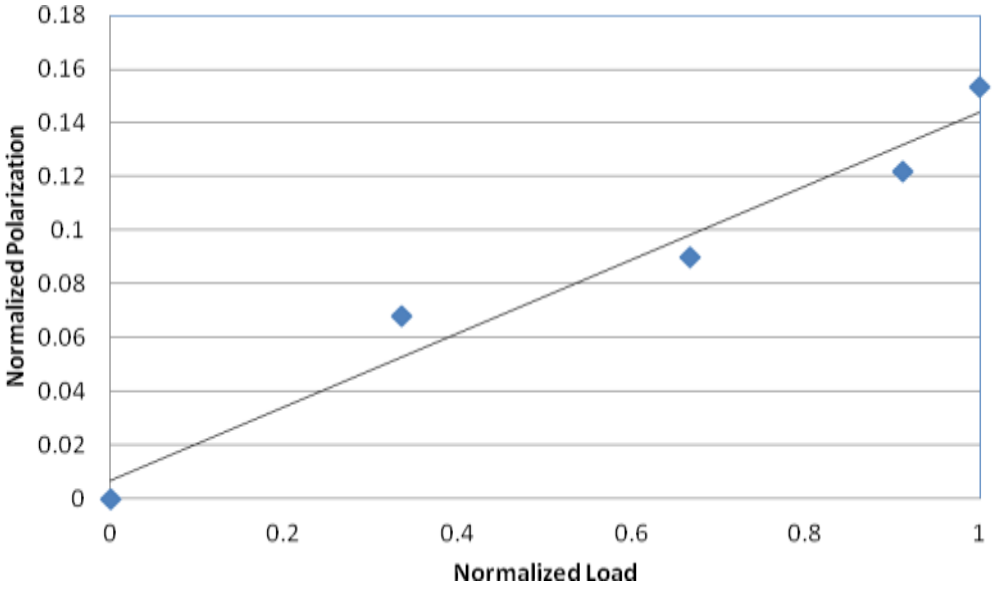

Fig. 25 – Normalized polarization Vs. Normalized load (dots) with its trendline (solid line)

The experiment at TTCI shows that the Rayleigh wave polarization depends on the longitudinal force of the rail. However, further research is recommended in order to solve the inverse problem, where the longitudinal force in the rail can be determined from the polarization of the Rayleigh wave. Follow on investigations are suggested to study the effect of the rail surface quality (polishing, sanding, grinding, blasting etc.) on the measured results. It would be useful to further investigate the effect of focusing of the laser vibrometer.

The design, manufacturing and thorough testing of a prototype would be the next step. Thereby, potential funding by Transportation Technology Center Inc. (TTCI) and Southwest University Transportation Center (SWUTC) is considered.

CHAPTER 6
Conclusions

This research investigated a method of determining the stress in rails by using the polarization of Rayleigh waves. The relationship between the polarization of Rayleigh waves and the state of stress is developed from the analytical model. The numerical simulation showed that the change of polarization of Rayleigh wave on residual stress is one order of magnitude higher than the change of Rayleigh wave speed. Additionally, sensitivity analysis showed that the polarization of a Rayleigh wave is more robust against uncertainties in material properties. These results concluded that Rayleigh wave polarization is more sensitive and more robust than the Rayleigh wave speed. These are the two main reasons why Rayleigh wave polarization was used instead of Rayleigh wave speed.

This method is a non-destructive and non-labor intensive measurement technique. The measurement of polarization is a point wise measurement, meaning that the applied stress on rail can be determined just by measuring the polarization from a single point. This method is also a reference-free measurement. No information about the propagation distance is needed to perform the measurement. The combination of these benefits is the advantage of this method that other methods do not have.

The results of the numerical simulation were verified with the preliminary experimental results. Further measurements were done in a stressed rail and the change in polarization of the Rayleigh wave was determined using a wedge transducer for generation and a laser Doppler vibrometer for the detection of ultrasonic waves. After a thorough evaluation, the concept was tested at Transportation Technology Center, Inc. (TTCI) facilities in Pueblo, CO, to transfer the developed technology to TTCI researches and Association of American Railroads (AAR) members. The results showed that the polarization of Rayleigh wave changes with longitudinal stress. Knowing the longitudinal stress will prevent future buckling of the rail and reduce the number of derailments and increase railroad safety.

The design, manufacturing and thorough testing of a prototype will be the next step. Thereby, potential funding by Transportation Technology Center Inc. (TTCI) and Southwest University Transportation Center (SWUTC) is considered.

REFERENCES

D. M. Egle and E. D. Bray (1976): Measurement of acousto-elastic and third-order elastic constants for rail steel, *Journal of the Acoustical Society of America*, Vol. 60, pp. 741-744.

D. M. Egle and E. D. Bray (1979): Application of the Acousto-Elastic Effect to Rail Stress Measurements. *Material Evaluation,* Vol. 37, pp. 41-55.

D. Read, B. Shust (2007). Railway Track & Structures. New York: Jun 2007. Vol. 103(6), pp. 19.

M. Junge. Measurement of Applied Stresses Using the Polarization of Rayleigh Surface Waves, *M.S. Thesis*. University of Stuttgart: November 2003.

M. Junge, and J. Qu, and L. J. Jacobs (2006): Relationship Between Rayleigh Wave Polarization and State of Stress, *Ultrasonics Journal*, Vol. 44(3), pp. 233-237.

D. I. Crecraft (1962): Ultrasonic wave velocities in stresses nickel steel, *Nature*, Vol. 195(4847), pp.1193.

D. I. Crecraft (1967): The Measurement of Applied and Residual Stresses in Metals for Measurement of Contained Stress in Railroad Rail, *Journal and Sound Vibration*, Vol. 5(1), pp. 173-192.

A. Kish and G. Samavedam (2005): Improved Destressing of Continuous Welded Rail for Better Management of Rail Neutral Temperature, *Journal of the Transportation Research Board,* Vol.1916, pp. 56-65.

A. Kish and D. Read (2006): Proceedings of the Workshop on CWR Track Stability, *Pueblo CO, March 15, 2006*

V. Damljanovic and R.L. Weaver (2005): Laser vibrometer technique for measurement of contained stress in railroad rail, *Journal of Sound and Vibration*, Vol.282, pp. 341-366.

M. Duquennoy, and M.Ouaftough, and M.Ourak (1999): Ultrasonic Evaluation of Stresses in Orthotropic Materials Using Rayleigh Waves, *NDT&E International*, Vol. 32(4), pp. 189-199.

M. Duquennoy, and M.Ouaftough, and M.L.Qian, F.Jenot and M.Ourak (2001): Ultrasonic Characterization of Residual Stresses in Steel Rods Using a Laser Line Source and Piezoelectric Transducers, *NDT&E International*, Vol. 34(5), pp. 355-362.

S. Hurlebaus (1996): Laser Generation and Detection Techniques for Developing Transfer Functions to Characterize the Effect of Geometry on Elastic Wave Propagation, *M.S. thesis, School of Civil and Environmental Engineering, Georgia Institute of Technology, Atlanta, GA.*

S. Hurlebaus (2002a): A Contribution to Structural Health Monitoring Using Elastic Waves, *PhD thesis, Institute A of Mechanics, University of Stuttgart, Stuttgart, Germany*

S. Hurlebaus (2002b): Laser Ultrasonics for Structural Health Monitoring, *Contribution to the 7th Laser-Vibrometer Seminar, Polytec, Waldbronn, Vol. 1 , pp. 1-27.*

S. Hurlebaus and L.J. Jacobs (2006): Dual Probe Laser Interferometer for Structural Health Monitoring, *Journal of the Acoustical Society of America,* Vol. 119(4), pp. 1923-1925.

M. Hirao, M. and H. Fukuoka, H. and K. Hori (1981): Acoustoelastic Effect of Rayleigh Surface Wave in Isotropic Material, *Journal of Applied Mechanics,* Vol. 48, pp. 119-124.

Y. H. Pao, and W. Sachse, and H.Fukuoka, (1984): Acoustoelasticity and Ultrasonic Measurements of Residual Stresses, *Physical Acoustics,* Vol. 17, pp. 61-143.

F. D. Murnaghan (1951). Finite Deformation of an Elastic Solid, Wiley, New York.

J. L. Rose (1999). *Ultrasonic Waves in Solid Media*. Cambridge University Press.

D. S. Hughes and J. L. Kelly. Second-Order Elastic Deformation of Solids. *Physical Review*, Vol. 92(5), pp. 1145-1149. December 1953.

R.T. Smith, R. Stern, and R.W.B. Stephens (1966). Third-Order Elastic Moduli of Polycrystalline Metals from Ultrasonic Velocity Measurements. *Journal of the Acoustical Society of America,* Vol. 40(5), pp. 1002-1008.

R.A. Toupin and B. Bernstein (1961). Sound Waves in Deformed Perfectly Elastic Materials. Acoustoelastic Effect. *Journal of the acoustical Society of America*, Vol. 33(2), pp. 216-225.

Y. H. Pao and U. Gamer (1985). Acoustoelastic Waves in Orthotropic Media. *Journal of the Acoustical Society of America*, Vol. 77(3), pp. 806.

B. Masserey and P. Fromme (2008). On The Reflection of Coupled Rayleigh-like Waves At Surface Defects in Plates, *Journal of the Acoustical Society of America*, Vol. 123, pp. 88 - 98.

I.A. Viktorov (1966). *Rayleigh and Lamb Waves*. Plenum Press, New York, NY.

K.F. Graff (1991). *Wave Motion in Elastic Solids*. Dover Publications Inc., New York.

H. G. Kil, J. Jarzynski, and Y. H. Berthelot (1998). Wave Decomposition of The Vibrations of A Cylindrical Shell With An Automated Scanning Laser Vibrometer. *Journal of the acoustical Society of America*, Vol. 104(6), pp. 3161-3168.

INVESTIGATOR PROFILE

Dr. Hurlebaus, Assistant Professor at Texas A&M University, is the Principal Investigator. His contact information is:

Dr.-Ing. Stefan Hurlebaus
Zachry Department of Civil Engineering
Texas Transportation Institute (TTI)
Texas A&M University
3136 TAMU
College Station, TX 77843-3136
USA
phone: (979) 845-9570
fax: (979) 845-6554
email: shurlebaus@civil.tamu.edu